

Analysis of anomalous transport with temporal fractional transport equations in a bounded domain

Kaibang Wu(吴凯邦), Jiayan Liu(刘嘉言), Shijie Liu(刘仕洁), Feng Wang(王丰), Lai Wei(魏来), Qibin Luan(栾其斌), and Zheng-Xiong Wang(王正汹)

Citation: Chin. Phys. B, 2023, 32 (**11**): 110502. DOI: 10.1088/1674-1056/acedf3
Journal homepage: http://cpb.iphy.ac.cn; http://iopscience.iop.org/cpb

What follows is a list of articles you may be interested in

Inatorial forecasting method considering macro and micro characteristics of chaotic traffic flow

Yue Hou(侯越), Di Zhang(张迪), Da Li(李达), and Ping Yang(杨萍)
Chin. Phys. B, 2023, 32 (**10**): 100508. DOI: 10.1088/1674-1056/acd3df

Current bifurcation, reversals and multiple mobility transitions of dipole in alternating electric fields

Wei Du(杜威), Kao Jia(贾考), Zhi-Long Shi(施志龙), and Lin-Ru Nie(聂林如)
Chin. Phys. B, 2023, 32 (**2**): 020505. DOI: 10.1088/1674-1056/ac7dbe

Solutions and memory effect of fractional-order chaotic system: A review

Shaobo He(贺少波), Huihai Wang(王会海), and Kehui Sun(孙克辉)
Chin. Phys. B, 2022, 31 (**6**): 060501. DOI: 10.1088/1674-1056/ac43ae

Uphill anomalous transport in a deterministic system with speed-dependent friction coefficient

Wei Guo(郭伟), Lu-Chun Du(杜鲁春), Zhen-Zhen Liu(刘真真), Hai Yang(杨海), Dong-Cheng Mei(梅冬成)
Chin. Phys. B, 2017, 26 (**1**): 010502. DOI: 10.1088/1674-1056/26/1/010502

Anomalous transport in fluid field with random waiting time depending on the preceding jump length

Hong Zhang(张红), Guo-Hua Li(李国华)
Chin. Phys. B, 2016, 25 (**11**): 110504. DOI: 10.1088/1674-1056/25/11/110504

Analysis of anomalous transport with temporal fractional transport equations in a bounded domain

Kaibang Wu(吴凯邦), Jiayan Liu(刘嘉言), Shijie Liu(刘仕洁), Feng Wang(王丰), Lai Wei(魏来), Qibin Luan(栾其斌), and Zheng-Xiong Wang(王正汹)[†]

Key Laboratory of Materials Modification by Beams of Ministry of Education, School of Physics, Dalian University of Technology, Dalian 116024, *China*

(Received 16 May 2023; revised manuscript received 12 July 2023; accepted manuscript online 8 August 2023)

Anomalous transport in magnetically confined plasmas is investigated using temporal fractional transport equations. The use of temporal fractional transport equations means that the order of the partial derivative with respect to time is a fraction. In this case, the Caputo fractional derivative relative to time is utilized, because it preserves the form of the initial conditions. A numerical calculation reveals that the fractional order of the temporal derivative α ($\alpha \in (0,1)$, sub-diffusive regime) controls the diffusion rate. The temporal fractional derivative is related to the fact that the evolution of a physical quantity is affected by its past history, depending on what are termed memory effects. The magnitude of α is a measure of such memory effects. When α decreases, so does the rate of particle diffusion due to memory effects. As a result, if a system initially has a density profile without a source, then the smaller the α is, the more slowly the density profile approaches zero. When a source is added, due to the balance of the diffusion and fueling processes, the system reaches a steady state and the density profile does not evolve. As α decreases, the time required for the system to reach a steady state increases. In magnetically confined plasmas, the temporal fractional transport model can be applied to off-axis heating processes. Moreover, it is found that the memory effects reduce the rate of energy conduction and hollow temperature profiles can be sustained for a longer time in sub-diffusion processes than in ordinary diffusion processes.

Keywords: anomalous transport, temporal fractional transport equation, Caputo fractional derivatives, memory effects, hollow temperature profiles

PACS: 05.60.–k, 05.70.Ln, 47.27.T–, 45.10.Hj **DOI:** 10.1088/1674-1056/acedf3

1. Introduction

The mechanism of anomalous particle transport is one of the most significant issues in magnetically confined plasmas. In ordinary transport theory, the Brownian random walk model states that interactions between particles occur via collisions, which can be modeled by the Langevin equation. With the assumption that random forces are independent of the particle displacements r, the solution to the Langevin equation gives $\langle r^2 \rangle \sim t$, meaning that the mean square displacement is linearly dependent on time t. However, in recent years, anomalous transport with a scaling law $\langle r^2 \rangle \sim t^\beta$ ($\beta \neq 1$) has been observed in many experiments and simulations.[1–7] The value of β can represent different processes: $0 < \beta < 1$ for sub-diffusion, $\beta = 1$ for ordinary diffusion, and $1 < \beta < 2$ for super-diffusion. Sub- and super-diffusions refer to particles diffusing more slowly and more quickly than in ordinary diffusion.

In magnetically confined plasmas, the Brownian random walk model based on collisions fails to explain experimental results due to collective behavior arising from the Coulomb force. In ordinary transport theory, the scaling law is $D \propto 1/B^2$,[8] where D is the diffusion coefficient and B is the magnitude of the magnetic field. However, Bohm experimentally determined the scaling law of diffusion to be $D \propto 1/B$,[9] which can be theoretically derived using the two-dimensional guiding center model.[10,11] In this model, due to the $\boldsymbol{E} \times \boldsymbol{B}$ drift motion of the guiding center, the velocity correlation can be transformed into an electric field correlation, which implies that the Coulomb force influences the diffusion process.

In Refs. [12–15], the decorrelation trajectory (DCT) method was proposed as a method to calculate diffusion coefficients. In this method, a global ensemble is divided into many sub-ensembles. In each sub-ensemble, the fluctuating electrostatic potential $\phi(\boldsymbol{x},t)$ has a fixed value at the starting point, i.e., at $\boldsymbol{x} = 0$ and at $t = 0$, and therefore the velocity of the guiding center of each sub-ensemble is expressed as $\nabla\phi(0,0) \times \boldsymbol{e}_z$ as a result of $\boldsymbol{E} \times \boldsymbol{B}$ drift. Furthermore, in each sub-ensemble, the decorrelation trajectory can be determined from the Hamiltonian equations of motion, along which the Eulerian correlation is calculated. Assuming that the Lagrangian velocity correlation in the sub-ensemble is equal to the Eulerian correlation, the diffusion coefficients can be calculated from the Lagrangian velocity correlation and related to the Kubo number defined as $K \equiv V\tau_c/\lambda_c$, where V, τ_c, and λ_c are the typical velocity of the particles, the correlation time, and the correlation length, respectively. Utilizing the DCT method yields $D \propto K^2$ for $K \ll 1$, and $D \propto K^\gamma$, $\gamma < 1$ for $K \gg 1$. When the guiding center is undergoing $\boldsymbol{E} \times \boldsymbol{B}$ drift motion,

[†]Corresponding author. E-mail: zxwang@dlut.edu.cn

© 2023 Chinese Physical Society and IOP Publishing Ltd

the Kubo number can be written as $K = \varepsilon\tau_c/(B\lambda_c^2)$, where ε is the amplitude of electrostatic potential fluctuations. Therefore, $K \gg 1$ implies that the system has strong turbulence due to the large amplitude of potential fluctuations. As particles encounter strong potential fluctuations, they are trapped by the fluctuations and undergo periodic motion.[12,16] As a result, it is possible that they diffuse more slowly than in the ordinary model and the system is in a sub-diffusive process.

In Refs. [12,17], the hybrid kinetic equations are utilized to obtain the evolution of the density profile,

$$\frac{\partial n(\boldsymbol{x},t)}{\partial t} = \int_0^t \mathrm{d}\tau L(\tau)\nabla^2 n(\boldsymbol{x},t-\tau), \tag{1}$$

where $L(\tau)$ is the Lagrangian velocity correlation. For an ordinary transport process, the amplitude of the fluctuation is small, implying $K \ll 1$. Utilizing the DCT method yields $L(\tau) \approx (\varepsilon/B\lambda_c)^2\,\mathrm{e}^{-\tau/\tau_c}$ such that the velocity correlation has an exponential decay and becomes insignificant as $\tau > \tau_c$. Since τ_c can be thought of as a short time scale, $n(\boldsymbol{x},t-\tau) \approx n(\boldsymbol{x},t)$ can be assumed if $t \gg \tau_c$, meaning that the density profile at time t does not relate to its past history. However, for an anomalous transport process, strong turbulence with large amplitude of fluctuation ($K \gg 1$) has significant effect on particle motions, then the DCT method gives $L(t) \sim t^{-\gamma}$ $(1 < \gamma < 2)$ stating that the velocity correlation has power law decay and the assumption $n(\boldsymbol{x},t-\tau) \approx n(\boldsymbol{x},t)$ is no longer applicable. Thus, the density profile at time t is influenced by its past history as illustrated on the right-hand side of Eq. (1), implying that memory effects do exist. Moreover, due to $L(t) \sim t^{-\gamma}$, manipulating the integration in Eq. (1) yields scaling law $\langle r^2\rangle \sim t^{\alpha}$ $(\alpha = 2-\gamma)$.[12,17] Hence, the density evolution of an anomalous transport process can be modeled by the temporal fractional diffusion equation.

Mathematically, the fractional derivatives are expressed as specific forms of integro-differential operators[18–20] that generalize the definition of conventional differentiation. There are many different types of fractional derivatives, including Riemann–Liouville, Grünwald–Letnikov, and Caputo derivatives. In our work, we utilize the Caputo fractional derivative[21]

$$\frac{\mathrm{d}^\alpha f}{\mathrm{d}t^\alpha} = \frac{1}{\Gamma(1-\alpha)}\int_0^t \frac{1}{(t-s)^\alpha}\frac{\mathrm{d}f}{\mathrm{d}s}\mathrm{d}s, \quad 0 < \alpha < 1, \tag{2}$$

where $\Gamma(x)$ is the Gamma function. It can be proven that the above formula returns to an ordinary first-order derivative as $\alpha \to 1$. The Caputo fractional derivative is useful for solving initial value problems because it preserves the form of the initial conditions. Theoretical methods for solving ordinary fractional differential equations with the Caputo fractional derivatives are summarized in Ref. [20]. The development of a numerical method to calculate Caputo fractional derivatives is significant to the study of complex problems as well. The Grünwald–Letnikov formula[19] and L1 formula[22] are the two main numerical formulae used to calculate Caputo fractional derivatives. If $0 < \alpha < 1$, the Grünwald–Letnikov formula can be used to obtain the first-order accuracy[19] and the L1 formula can improve the accuracy of order $2-\alpha$.[23] In Ref. [24], the L1-2 formula was used to achieve an accuracy of order $3-\alpha$ by means of quadratic interpolation. The algorithms of numerical solution to other types of temporal fractional derivatives are discussed in Ref. [25] to investigate the memory effects in fractional-order chaotic systems.

The temporal fractional transport model in cylindrical coordinates has been studied in recent years in other academic fields.[26–31] In Ref. [12], the solution to the evolution of a density profile in an infinite domain in cylindrical coordinates in the absence of a source was derived. However, in real tokamaks, plasma particles are confined in a bounded domain and the solution to the diffusion equation can be expanded in terms of a series of orthogonal functions. In our work, we assume that a plasma system encounters a non-Markovian process with strong turbulence in a bounded domain. As mentioned in Refs. [12,16], plasma particles in a system with strong turbulence will be trapped by electric fields generated by large fluctuations. As a result, plasma particles diffuse slowly than ordinary. This kind of anomalous transport can be modeled using temporal fractional transport equations. Therefore, the goal of this work is to investigate memory effects on transport through numerical and analytical methods in a bounded domain. This paper is organized as follows: Section 2 briefly reviews the derivation of the temporal fractional diffusion equations. Section 3 compares the numerical results of density profiles under various orders of temporal fractional derivatives without sources and with uniform sources. At the end of Section 3, the application to off-axis heating processes is discussed. Section 4 presents a theoretical analysis, and Section 5 contains the summary and conclusions.

2. Derivation of the temporal fractional transport equation

In an ordinary transport process, particle jumps occur at regular, well-defined time intervals. However, in real situations, the time interval between successive jumps varies. Therefore, the continuous time random walk (CTRW) model can be introduced to generalize the Brownian random walk model.[32] In this model, particles are allowed to have an arbitrary jump length and waiting time expressed by probability distribution functions (PDFs). Furthermore, the temporal fractional diffusion equation can be derived from the master equation of this model.[33] In this paper, we concisely review the

derivation of the temporal fractional transport equation from the CTRW model and the detailed derivation processes are provided in Refs. [12,32,33]. Suppose that a particle is at position $\boldsymbol{x}'$ at time t', then stays at $\boldsymbol{x}'$ during a waiting time $t-t'$, and then jumps to position $\boldsymbol{x}$. We define $f(\boldsymbol{x}-\boldsymbol{x}')$ as the PDF of the jump $\boldsymbol{x}-\boldsymbol{x}'$ and $\psi(t-t')$ as the PDF of the waiting time $t-t'$, such that the PDF of the process can be expressed as $\xi(\boldsymbol{x}-\boldsymbol{x}',\boldsymbol{x}';t-t';t') = f(\boldsymbol{x}-\boldsymbol{x}')\psi(t-t')$. We further denote $\tilde{w}$ as the Laplace transform of function w and $\hat{v}$ as the Fourier transform of function v through

$$\tilde{w}(\boldsymbol{x},p) = \int_0^\infty w(\boldsymbol{x},t)\mathrm{e}^{-pt}\mathrm{d}t,$$
$$\hat{v}(\boldsymbol{k},t) = \int_{-\infty}^\infty v(\boldsymbol{x},t)\mathrm{e}^{\mathrm{i}\boldsymbol{k}\cdot\boldsymbol{x}}\mathrm{d}\boldsymbol{x}.$$

Defining $\tilde{\phi} \equiv p\tilde{\psi}/(1-\tilde{\psi})$, we have

$$\frac{\partial n(\boldsymbol{x},t)}{\partial t} = \int \mathrm{d}x' f(\boldsymbol{x}-\boldsymbol{x}') \int_0^t \mathrm{d}t' \phi(t-t') n(\boldsymbol{x}',t') - \int_0^t \mathrm{d}t' \phi(t-t') n(\boldsymbol{x},t'). \tag{3}$$

Taking the Laplace transform in time and the Fourier transform in space of Eq. (3) yields

$$\hat{\tilde{n}}(\boldsymbol{k},p) = \frac{\hat{n}_0(\boldsymbol{k})}{p-\tilde{\phi}(p)[\hat{f}(\boldsymbol{k})-1]} = \frac{1-\tilde{\psi}(p)}{p[1-\tilde{\psi}(p)\hat{f}(\boldsymbol{k})]}\hat{n}_0(\boldsymbol{k}), \tag{4}$$

where the initial condition $n_0(\boldsymbol{x})\delta(t)$ is assumed. From the statistical definition of average, we may write

$$\hat{f}(\boldsymbol{k}) = \int_{-\infty}^\infty f(\boldsymbol{x})\mathrm{e}^{\mathrm{i}\boldsymbol{k}\cdot\boldsymbol{x}}\mathrm{d}\boldsymbol{x} = \langle \mathrm{e}^{\mathrm{i}\boldsymbol{k}\cdot\boldsymbol{x}}\rangle = 1 + \mathrm{i}\boldsymbol{k}\cdot\langle\boldsymbol{x}\rangle - \frac{1}{2}\boldsymbol{k}\boldsymbol{k}:\langle\boldsymbol{x}\boldsymbol{x}\rangle + O(k^3), \tag{5}$$

$$\tilde{\psi}(p) = \int_0^\infty \psi(t)\mathrm{e}^{-pt}\mathrm{d}t = \langle \mathrm{e}^{-pt}\rangle = 1 - p\langle t\rangle + O(p^2), \tag{6}$$

where $\langle\cdots\rangle$ denotes the statistical average. Therefore, from Eq. (6) we have

$$\langle t\rangle = -\frac{\mathrm{d}\tilde{\psi}(p)}{\mathrm{d}p}\Big|_{p=0}. \tag{7}$$

Moreover, since the directions of jumps are randomly distributed, we have $\langle\boldsymbol{x}\rangle = 0$ and Eq. (5) becomes

$$\hat{f}(\boldsymbol{k}) = \int_{-\infty}^\infty f(\boldsymbol{x})\mathrm{e}^{\mathrm{i}\boldsymbol{k}\cdot\boldsymbol{x}}\mathrm{d}\boldsymbol{x} = \langle \mathrm{e}^{\mathrm{i}\boldsymbol{k}\cdot\boldsymbol{x}}\rangle = 1 - \frac{1}{2}\boldsymbol{k}\boldsymbol{k}:\langle\boldsymbol{x}\boldsymbol{x}\rangle + O(k^3). \tag{8}$$

In one-dimensional space with the fluid limit ($k\to 0$, $s\to 0$), we assume that the system has a characteristic time τ_c and a characteristic length λ_c implying $\langle t\rangle = \tau_\mathrm{c}$ and $\langle x^2\rangle = \lambda_\mathrm{c}^2$. Hence, we have $\tilde{\psi}(p) \approx 1-\tau_\mathrm{c}p$ and $\hat{f}(k) \approx 1-\lambda_\mathrm{c}^2k^2$. Substituting them into Eq. (4) gives

$$p\hat{\tilde{n}}(k,p) - \hat{n}_0(k) = -\frac{\lambda_\mathrm{c}^2}{\tau_\mathrm{c}}k^2\hat{\tilde{n}}(k,p). \tag{9}$$

Performing the inverse Laplace–Fourier transforms on Eq. (9) gives

$$\frac{\partial n(x,t)}{\partial t} = \frac{\lambda_\mathrm{c}^2}{\tau_\mathrm{c}}\nabla^2 n(x,t), n(x,0) = n_0(x),$$

which returns to the ordinary diffusion equation.

In a system with strong turbulence, particles will be trapped by fluctuation and have periodic motions. As a consequence, the PDF of waiting time $\psi(t)$ has a long tail such that $\langle t\rangle$ is infinite, implying that the system does not have characteristic time. In fact, assuming $\tilde{\psi}(p) = 1-\tau_\mathrm{c}^\alpha p^\alpha$ $(0<\alpha<1)$ yields $\langle t\rangle = -\mathrm{d}\tilde{\psi}(p)/\mathrm{d}p\big|_{p=0} = \alpha\tau_\mathrm{c}^\alpha p^{\alpha-1}\big|_{p=0} \to \infty$. Keeping the assumption $\hat{f}(\boldsymbol{k}) = 1-\lambda_\mathrm{c}^2k^2$, from Eq. (4) we obtain

$$p^\alpha\hat{\tilde{n}}(\boldsymbol{k},p) - p^{\alpha-1}\hat{n}_0(\boldsymbol{k}) = -\frac{\lambda_\mathrm{c}^2}{\tau_\mathrm{c}^\alpha}k^2\hat{\tilde{n}}(\boldsymbol{k},p). \tag{10}$$

Moreover, taking the Laplace transform of Eq. (2) yields

$$\int_0^\infty \frac{\mathrm{d}^\alpha f}{\mathrm{d}t^\alpha}\mathrm{e}^{-pt}\mathrm{d}t = \frac{1}{\Gamma(1-\alpha)}\int_0^\infty \mathrm{e}^{-pt}\mathrm{d}t\int_0^t \frac{1}{(t-s)^\alpha}\frac{\mathrm{d}f}{\mathrm{d}s}\mathrm{d}s = p^\alpha\tilde{f}(p) - p^{\alpha-1}f(0). \tag{11}$$

Utilizing Eq. (11) and performing the inverse Laplace–Fourier transform on Eq. (10), we have

$$\frac{\partial^\alpha n}{\partial t^\alpha} = D_\alpha\nabla^2 n, \tag{12}$$

where $D_\alpha = \lambda_\mathrm{c}^2/\tau_\mathrm{c}^\alpha$. Suppose that there is an additional source $S_\mathrm{add}(\boldsymbol{x},t)$, then the above equation becomes

$$\frac{\partial^\alpha n}{\partial t^\alpha} = D_\alpha\nabla^2 n + S_\mathrm{add}. \tag{13}$$

If $\alpha = 1$, the transport process is Markovian. If $0<\alpha<1$, the transport process is non-Markovian, and the memory effects have an influence on the transport process. In other words, α measures the influence level of the memory effects.

In Refs. [12,17], it was shown that the temporal fractional transport equation can be derived by the DCT method. Based on the DCT method, the asymptotic form of velocity correlation can be assumed to read $L(t) \approx A_0 t^{-\gamma}$ $(1<\gamma<2)$, where A_0 is a constant and Eq. (1) becomes

$$\frac{\partial n(\boldsymbol{x},t)}{\partial t} = \int_0^t \mathrm{d}\tau A_0\tau^{-\gamma}\nabla^2 n(\boldsymbol{x},t-\tau). \tag{14}$$

Taking the Laplace transform on Eq. (14), we have

$$s\tilde{n}(\boldsymbol{x},s) - n(\boldsymbol{x},0) = A_0 s^{\gamma-1}\Gamma(1-\gamma)\nabla^2\tilde{n}(\boldsymbol{x},s). \tag{15a}$$

Equation (15a) can be rewritten as

$$s^{2-\gamma}\tilde{n}(\boldsymbol{x},s)-s^{1-\gamma}n(\boldsymbol{x},0)=A_0\Gamma(1-\gamma)\nabla^2\tilde{n}(\boldsymbol{x},s). \quad (15b)$$

By performing the inverse Laplace transform yields

$$\frac{\partial^{2-\gamma}n}{\partial t^{2-\gamma}}=A_0\Gamma(1-\gamma)\nabla^2 n, \quad (16)$$

Eq. (16) is consistent with Eq. (12) if $\alpha=2-\gamma$ and $D_\alpha=A_0\Gamma(1-\gamma)$. Thus, the temporal fractional transport equation derived from the CTRW model is consistent with that derived from the DCT method.

3. Numerical results

In cylindrical coordinates, with a constant diffusion coefficient, the temporal fractional diffusion equation reads

$$\frac{\partial^\alpha n}{\partial t^\alpha}=\frac{D_\alpha}{r}\frac{\partial}{\partial r}\left(r\frac{\partial n}{\partial r}\right)+S_{\rm add}. \quad (17)$$

Note that the dimensionless variables are defined as $r/a\to r$, $t/t_0\to t$, $D_\alpha t_0^\alpha/a^2\to D_\alpha$, where D_α is the characteristic diffusion coefficient, a is the minor radius, and t_0 is the characteristic particle confinement time. Furthermore, the dimensionless variables of the source and the density are defined as $S_{\rm add}/S_0\to S_{\rm add}$ and $n/n_0\to n$, where n_0 is the characteristic diffusive scale of the density and $S_0=n_0/t_0^\alpha$ is the characteristic scale of the source. In Ref. [24], the authors developed the L1-2 formula, which expresses the temporal fractional partial derivative at time t_i at position r_j as

$$\frac{\partial^\alpha}{\partial t^\alpha}n_j^i\approx\frac{\Delta t^{-\alpha}}{\Gamma(2-\alpha)}\sum_{k=0}^{i-1}c_k^{(i,\alpha)}(n_j^{i-k}-n_j^{i-k-1}), \quad (18)$$

where $c_0^{(1,\alpha)}=1$ if $i=1$, and

$$\begin{aligned}
c_0^{(i,\alpha)}&=\frac{1}{2}+\frac{1}{2-\alpha},\\
c_k^{(i,\alpha)}&=\frac{(k+1)^{1-\alpha}-2k^{1-\alpha}+(k-1)^{1-\alpha}}{2}\\
&\quad+\frac{(k+1)^{2-\alpha}-2k^{2-\alpha}+(k-1)^{2-\alpha}}{2-\alpha},\quad 1\leqslant k\leqslant i-2,\\
c_{i-1}^{(i,\alpha)}&=\frac{(i-2)^{1-\alpha}-(i-1)^{1-\alpha}+2i^{1-\alpha}}{2}\\
&\quad-\frac{(i-1)^{2-\alpha}-(i-2)^{2-\alpha}}{2-\alpha}
\end{aligned}$$

if $i\geqslant 2$ and $\mathrm{i}\Delta t=t_i$. Since the authors utilized the explicit scheme for the temporal fractional partial differential equation, we apply the Crank–Nicholson method to improve the numerical stability in our work and the spatial partial derivative can be approximated as

$$\frac{D_\alpha}{r}\frac{\partial}{\partial r}\left(r\frac{\partial n}{\partial r}\right)\approx D_\alpha\left\{\frac{\left[r_{j+\frac{1}{2}}\left(n_{j+1}^i-n_j^i\right)-r_{j-\frac{1}{2}}\left(n_j^i-n_{j-1}^i\right)\right]+\left[r_{j+\frac{1}{2}}\left(n_{j+1}^{i-1}-n_j^{i-1}\right)-r_{j-\frac{1}{2}}\left(n_j^{i-1}-n_{j-1}^{i-1}\right)\right]}{2r_j(\Delta r)^2}\right\}, \quad (19)$$

where $r_j=j\Delta r$, $r_{j+\frac{1}{2}}=(2j+1)\Delta r/2$, $r_{j-\frac{1}{2}}=(2j-1)\Delta r/2$, $j=1,2,3,\ldots,n-1$, and $n\Delta r=1$. Thus, combining Eqs. (18) and (19) without a source yields

$$\begin{aligned}
&-\frac{2j+1}{4j}\frac{D_\alpha}{(\Delta r)^2}n_{j+1}^1+\left[\frac{\Delta t^{-\alpha}}{\Gamma(2-\alpha)}+\frac{D_\alpha}{(\Delta r)^2}\right]n_j^1\\
&-\frac{2j-1}{4j}\frac{D_\alpha}{(\Delta r)^2}n_{j-1}^1\\
=&\frac{2j+1}{4j}\frac{D_\alpha}{(\Delta r)^2}n_{j+1}^0+\left[\frac{\Delta t^{-\alpha}}{\Gamma(2-\alpha)}-\frac{D_\alpha}{(\Delta r)^2}\right]n_j^0\\
&+\frac{2j-1}{4j}\frac{D_\alpha}{(\Delta r)^2}n_{j-1}^0
\end{aligned} \quad (20)$$

if $i=1$, and

$$\begin{aligned}
&-\frac{2j+1}{4j}\frac{D_\alpha}{(\Delta r)^2}n_{j+1}^i+\left[\frac{\Delta t^{-\alpha}c_0^{(i,\alpha)}}{\Gamma(2-\alpha)}+\frac{D_\alpha}{(\Delta r)^2}\right]n_j^i\\
&-\frac{2j-1}{4j}\frac{D_\alpha}{(\Delta r)^2}n_{j-1}^i\\
=&\frac{2j+1}{4j}\frac{D_\alpha}{(\Delta r)^2}n_{j+1}^{i-1}+\left[\frac{\Delta t^{-\alpha}c_0^{(i,\alpha)}}{\Gamma(2-\alpha)}-\frac{D_\alpha}{(\Delta r)^2}\right]n_j^{i-1}\\
&+\frac{2j-1}{4j}\frac{D_\alpha}{(\Delta r)^2}n_{j+1}^{i-1}
\end{aligned}$$

$$-\frac{\Delta t^{-\alpha}}{\Gamma(2-\alpha)}\sum_{k=1}^{i-1}c_k^{(i,\alpha)}(n_j^{i-k}-n_j^{i-k-1}) \quad (21)$$

if $i\geqslant 2$. If there is a source, then $S_{{\rm add}\ j}^i$ will be added on the right-hand side of Eqs. (20) and (21). The total number of particles can be defined as

$$N_{\rm tot}(t)=2\pi\int_0^1 n(r,t)r{\rm d}r,$$

so that we can investigate the effect of α on the evolution of density profiles. Next, we numerically solve Eq. (13) with and without sources.

3.1. Without sources

We first investigate the diffusion rate for different temporal fractional orders α without a source and with a constant diffusion coefficient $D_\alpha=0.01$. In our simulation, the initial condition is $n(r,0)=1-r^2$ ($N_{\rm tot}(0)=\pi/2\approx 1.5708$), and the boundary conditions are $\partial n/\partial r\big|_{r=0}=n(1,t)=0$. Figure 1 shows the density profiles for different α at $t=200$ and $t=400$. In Fig. 1(a), the magnitudes of $N_{\rm tot}$ are approximately

1.2953 for $\alpha = 0.2$, and 0.1160 for $\alpha = 0.8$, which means that the total number of particles N_{tot} drops 17.54% and 92.62% from the initial conditions for $\alpha = 0.2$ and $\alpha = 0.8$, respectively. Hence, as α becomes larger, the density decays faster. Furthermore, the magnitude of N_{tot} is 1.2953 at $t = 200$, and 1.2681 at $t = 400$, for $\alpha = 0.2$, which means that the total number of particles decays faster at the beginning and then slows down.

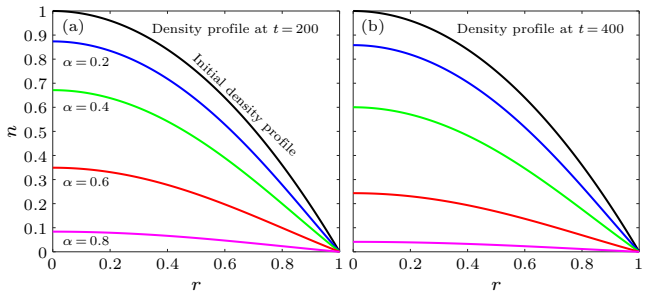


Fig. 1. Density profiles at times $t = 200$ and $t = 400$ without sources. Comparing the blue, green, red, and magenta curves at $t = 200$ and $t = 400$, it is found that a smaller α leads to slower particle diffusion. Thus, the value of α controls the diffusion rate of the density.

3.2. With uniform sources

Next, we investigate the evolution of density profiles with sources. In this situation, the particles diffuse and also increase in number due to the injection from the sources. As a result, the diffusion and source terms eventually balance out, so that the system arrives at a steady state. Hence, in the steady state we have

$$\frac{\partial^{\alpha} n}{\partial t^{\alpha}} = \frac{D_{\alpha}}{r}\frac{\partial}{\partial r}\left(r\frac{\partial n}{\partial r}\right) + S_{\text{add}} = 0, \tag{22}$$

which implies that the form of the density profile at the steady state n_{s} is independent of α and depends on S_{add}. We assume that the initial condition $n(r,0) = 0$ and that the source term is a constant, i.e., $S_{\text{add}} = \text{const}$. Therefore, the solution to Eq. (22) is

$$n_{\text{s}}(r) = \frac{S_{\text{add}}}{4D_{\alpha}}(1 - r^2). \tag{23}$$

Thus, in the steady state, $n_{\text{s}}(r) = (1 - r^2)/4$ and the total number of particles at steady state $N_{\text{s}} = \pi/8$ can be obtained if $D_{\alpha} = 0.01$ and $S_{\text{add}} = 0.01$ are assumed.

Figure 2 illustrates that all of the curves approach $n_{\text{s}}(r) = (1 - r^2)/4$ at different speeds depending on α. For instance, Fig. 2(d) reveals that the magnitude of N_{tot} for $\alpha = 0.8$ is larger than that for $\alpha = 0.2$, indicating that a larger α leads to a faster approach of the density profile toward $n_{\text{s}}(r)$. Moreover, from the magnitude of N_{tot} for each α at each moment, it is found that the density profiles grow faster at the beginning and then slow down. Detailed data are listed in Table 1.

Thus, the simulation reveals that as $\alpha \to 1$, the diffusion rate increases. As a result, the density decreases faster for $\alpha = 0.8$ than for $\alpha = 0.2$ without sources, and the density increases faster for $\alpha = 0.8$ than for $\alpha = 0.2$ with sources.

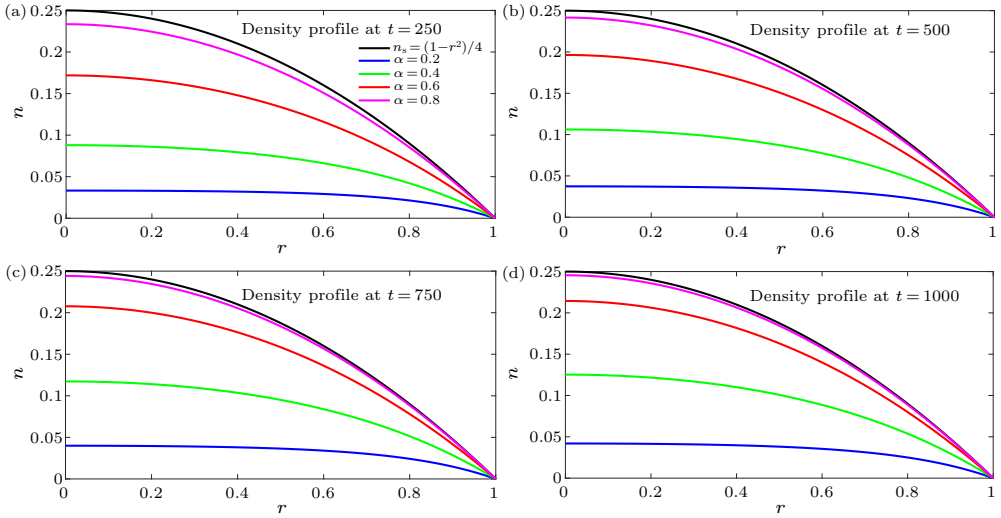


Fig. 2. The evolution of the density profiles at different moments and different α with $S_{\text{add}} = 0.01$. The black curves represent the density profile $n_{\text{s}}(r) = (1 - r^2)/4$ in the steady state and each curve approaches n_{s} with a different speed depending on α.

Table 1. The total number of particles N_{tot} at different moments.

	N_{tot} at $t = 250$	N_{tot} at $t = 500$	N_{tot} at $t = 750$	N_{tot} at $t = 1000$
$\alpha = 0.2$	0.0721	0.0792	0.0837	0.0870
$\alpha = 0.4$	0.1612	0.1884	0.2047	0.2162
$\alpha = 0.6$	0.2836	0.3179	0.3337	0.3431
$\alpha = 0.8$	0.3697	0.3811	0.3847	0.3865

3.3. Applications to magnetically confined plasmas

So far, as mentioned in Subsections 3.1 and 3.2, it is found that as the temporal fractional order α deceases, the rate of diffusion decreases as well. Therefore, α can be thought of as the measure of the memory effects. In the derivation of the temporal fractional transport equation, we start with the CTRW model of particles. Supposing that these particles carry energy, as they jump from position x' to position x during a waiting time $t-t'$, energy transport may occur. Therefore, we may utilize the CTRW model to simulate the evolution of the temperature profile and Eq. (8) can be rewritten as

$$\frac{\partial^\alpha T}{\partial t^\alpha} = \chi_\alpha \nabla^2 T + H_{\rm add}, \tag{24}$$

where T is the temperature, χ_α is the thermal conductivity, and $H_{\rm add}$ is the heating source. Hence, the memory effects on the anomalous transport of temperature can be investigated through Eq. (24). In early works, hollow temperature profiles were observed in steady states under off-axis heating,[34] and theories based on nonlocal transport by utilizing the spatial fractional transport equation in Markovian processes were developed.[35–38] In order to investigate memory effects on the formation of hollow temperature profiles under off-axis heating processes, we assume the heating source to be of the form $H_{\rm add} = H_{\rm e}{\rm e}^{-(r-r_0)^2/a^2}$, where $r_0 = 0.75$, $a = 0.05$, and $H_{\rm e}$ is a constant, such that

$$2\pi \int_0^1 H_{\rm add} r{\rm d}r = 2\pi H_{\rm e} \int_0^1 {\rm e}^{-(r-r_0)^2/a^2} r{\rm d}r = 1.$$

The initial and boundary conditions are the same as those in the above section. Figure 3 shows the evolution of temperature profiles for various α. In this work, the temperature profiles in the steady state $T_{\rm s}(r)$ can be obtained by solving $\chi_\alpha \nabla^2 T + H_{\rm add} = 0$ using the finite difference method.

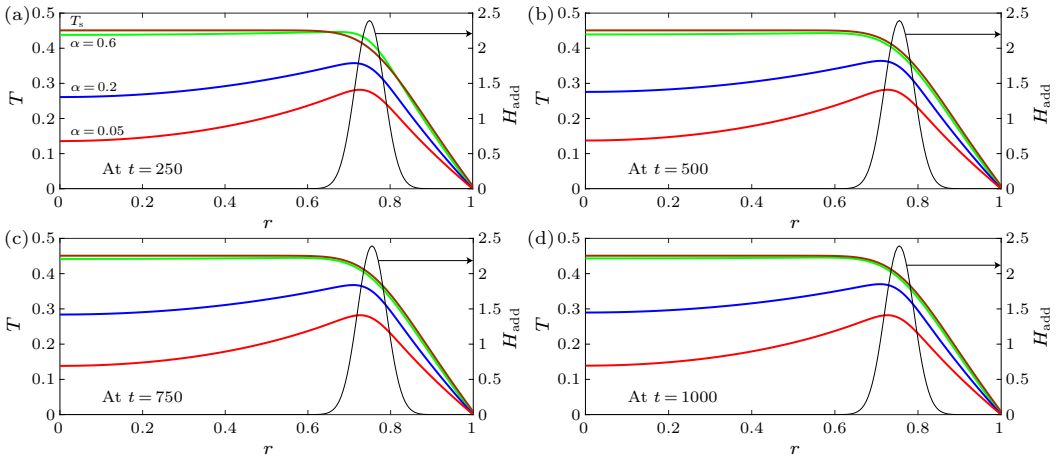


Fig. 3. When a plasma system is heated at its edge, a hollow temperature profile can result. In a steady state, the temperature profile $T_{\rm s}$ can be obtained using the finite difference scheme. However, for a system with α approaching zero, the memory effects weaken the heat conduction, such that the hollow temperature profile can be sustained for a longer time.

Table 2. The temperature spread $\varepsilon_{\rm e}(t)$ for different α at different moments.

	$\alpha = 0.6$	$\alpha = 0.2$	$\alpha = 0.05$
$\varepsilon_{\rm e}$ at $t = 250$	1.0572	0.7847	0.5579
$\varepsilon_{\rm e}$ at $t = 500$	1.0664	0.8062	0.5593
$\varepsilon_{\rm e}$ at $t = 750$	1.0702	0.8182	0.5601
$\varepsilon_{\rm e}$ at $t = 1000$	1.0724	0.8265	0.5607

When a plasma system undergoes an off-axis heating process, heat is first conducted from the location of the heating source. As shown in Fig. 3, heat in a system with $\alpha = 0.6$ is conducted faster than that with $\alpha = 0.2$ and $\alpha = 0.05$, such that the temperature profile from the core to $r_0 = 0.75$ for $\alpha = 0.6$ is flatter than that for $\alpha = 0.2$ and $\alpha = 0.05$. Moreover, it is found that temperature profiles have local minima at the core for each α and that the maxima are close to the position of the heating source. Hence, hollow temperature profiles are formed. In order to investigate memory effects on hollow temperature profiles, we further define the temperature spread $\varepsilon_{\rm e}(t)$ as

$$\varepsilon_{\rm e}(t) = 2\pi \int_0^1 T(r,t) r{\rm d}r, \tag{25}$$

and the simulation results are listed in Table 2.

In Table 2, it is seen that α controls the magnitude of the temperature spread $\varepsilon_{\rm e}(t)$. As α is close to zero, the increase rate of $\varepsilon_{\rm e}(t)$ decreases. For instance, $(\varepsilon_{\rm e}|_{t=1000} - \varepsilon_{\rm e}|_{t=750})/250 \approx 8.8 \times 10^{-6}$ for $\alpha = 0.6$, and $(\varepsilon_{\rm e}|_{t=1000} - \varepsilon_{\rm e}|_{t=750})/250 \approx 2.4 \times 10^{-6}$ for $\alpha = 0.05$. Hence, the memory effects impede heat conduction. In Fig. 3 it is found that the hollow temperature profile can be observed until the profile is consistent with the profile $T_{\rm s}$ in the steady state. However, if we take the hollow temperature profile for $\alpha = 0.05$ as the object of study, due to the fact that the increase rate of $\varepsilon_{\rm e}(t)$ from $t = 250$ to $t = 1000$ is

$(\varepsilon_e|_{t=1000} - \varepsilon_e|_{t=250})/750 \approx 3.7 \times 10^{-6} \ll 1$ for $\alpha = 0.05$, the system can be considered to be in a quasi-static state. Hence, the hollow temperature profiles can be observed for a long time due to the memory effects.

4. Theoretical analysis

To solve Eq. (13) without a source, we assume that the diffusion coefficient is a constant, the initial condition is $n(r,0) = f(r)$, and the boundary conditions are $\partial n/\partial r|_{r=0} = n(1,t) = 0$. Applying the method of separation of variables, we obtain the solution to Eq. (13) as follows:

$$n(r,t) = \sum_{n=1}^{\infty} A_n E_{\alpha,1}(-D_\alpha r_n^2 t^\alpha) J_0(r_n r), \tag{26}$$

where $E_{\alpha,\beta}(z)$ is the Mittag–Leffler function, defined as

$$E_{\alpha,\beta}(z) = \sum_{k=0}^{\infty} \frac{z^k}{\Gamma(\alpha k + \beta)}, \tag{27}$$

and $J_0(x)$ and $J_1(x)$ are the Bessel functions of the first kind of orders 0 and 1, respectively; r_n are specific values such that $J_0(r_n) = 0$. Substituting it in the initial condition and utilizing the orthogonality of the Bessel functions, we have

$$A_n = \frac{2}{J_1^2(r_n)} \int_0^1 r f(r) J_0(r_n r) \mathrm{d}r. \tag{28}$$

When the additional source as a function of space and time $S_{\mathrm{add}}(r,t)$ is taken into account, the solution can be assumed to have the form

$$n(r,t) = \sum_{n=1}^{\infty} T_n(t) J_0(r_n r), \tag{29}$$

and the source term can be expanded through the Bessel functions

$$S_{\mathrm{add}}(r,t) = \sum_{n=1}^{\infty} B_n(t) J_0(r_n r). \tag{30}$$

Therefore, the orthogonality of the Bessel functions gives

$$T_n(t) = \frac{2}{J_1^2(r_n)} \int_0^1 r n(r,t) J_0(r_n r) \mathrm{d}r, \tag{31}$$

$$B_n(t) = \frac{2}{J_1^2(r_n)} \int_0^1 r S_{\mathrm{add}}(r,t) J_0(r_n r) \mathrm{d}r. \tag{32}$$

Taking an α-order derivative with respect to time for both sides of Eq. (31) and utilizing Eq. (13) with the initial and boundary conditions, we obtain

$$\frac{\mathrm{d}^\alpha T_n}{\mathrm{d}t^\alpha} = -r_n^2 D_\alpha T_n + B_n.$$

The solution to the above equation can be derived through the Laplace transform. Therefore, we have

$$T_n(t) = A_n E_{\alpha,1}(-D_\alpha r_n^2 t^\alpha) + \int_0^t B_n(s)(t-s)^{\alpha-1} E_{\alpha,\alpha}[-D_\alpha r_n^2 (t-s)^\alpha] \mathrm{d}s.$$

Thus, the solution to Eq. (13) reads

$$n(r,t) = \sum_{n=1}^{\infty} J_0(r_n r) \Big\{ A_n E_{\alpha,1}(-D_\alpha r_n^2 t^\alpha) + \int_0^t B_n(s)(t-s)^{\alpha-1} E_{\alpha,\alpha}[-D_\alpha r_n^2 (t-s)^\alpha] \mathrm{d}s \Big\}. \tag{33}$$

The first term in the braces on the right-hand side of Eq. (33) is the solution in the absence of an additional source term, while the second term represents the effect of the additional source term on the solution. Moreover, Eq. (33) reveals that the solution can be expanded in a series of Bessel functions, unlike the solution for an unbounded domain derived in Ref. [12]. If $\alpha \to 1$, Eq. (13) returns to an ordinary diffusion equation and Eq. (33) becomes

$$n(r,t) = \sum_{n=1}^{\infty} J_0(r_n r) \Big\{ A_n \exp(-D_\alpha r_n^2 t) + \int_0^t B_n(s) \exp[-D_\alpha r_n^2 (t-s)] \mathrm{d}s \Big\},$$

which is consistent with the solution to the ordinary diffusion equation.

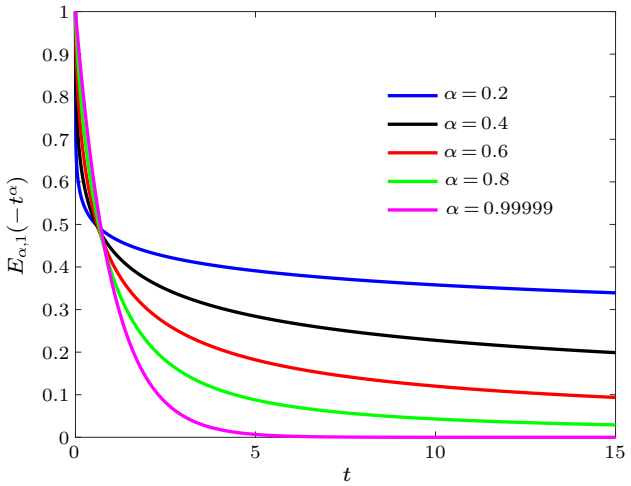


Fig. 4. The decay of the function $E_{\alpha,1}(-t^\alpha)$ with time for different α. The slopes of all curves are steep in the beginning and then become shallower. This is consistent with the simulation results, showing that the total number of particles decreases rapidly at the beginning and more slowly at later times.

We next study the situation without an additional source, so the second term on the right-hand side of Eq. (33) can be ignored. Then the solution reads

$$n(r,t) = \sum_{n=1}^{\infty} A_n J_0(r_n r) E_{\alpha,1}(-D_\alpha r_n^2 t^\alpha). \tag{34}$$

To investigate the effect of α on the evolution of the density profile, we may set $D_\alpha r_n^2 = 1$ for simplicity. Figure 4 shows that as time increases, $E_{\alpha,1}(-t^\alpha)$ decreases and eventually approaches zero. Moreover, it is found that the rate of

decay depends on α. For instance, at $t=7$, for $\alpha=0.99999$, $E_{\alpha,1}(-t^\alpha)\approx 0$, while for $\alpha=0.2$, $E_{\alpha,1}(-t^\alpha)\approx 0.375$. Hence, as α increases, the decay rate of the density increases as well.

The asymptotic behavior of the Mittag–Leffler function is

$$E_{\alpha,\beta}(z)=-\sum_{k=1}^{N}\frac{z^{-k}}{\Gamma(\beta-\alpha k)}+O(z^{-N-1}), \tag{35}$$

where $|z|\to\infty$, $\pi\alpha/2<\mu<\min[\pi,\pi\alpha]$, and $\mu\leqslant|\arg(z)|\leqslant\pi$.[20] Therefore, as $t\to\infty$ we may truncate Eq. (35) to the first term

$$E_{\alpha,1}(-t^\alpha)=\sum_{k=1}^{N}\frac{(-1)^{1-k}t^{-\alpha k}}{\Gamma(1-\alpha k)}\approx\frac{t^{-\alpha}}{\Gamma(1-\alpha)}.$$

Since A_n and $J_0(r_n r)$ are independent of time, according to Eq. (34), as $E_{\alpha,1}(-D_\alpha r_n^2 t^\alpha)\to 0$, $n(r,t)\to 0$, we may define the truncation time $t_{\rm trun}$ such that $E_{\alpha,1}(-t_{\rm trun}^\alpha)=0.01$. Therefore,

$$t_{\rm trun}=\left[\frac{100}{\Gamma(1-\alpha)}\right]^{1/\alpha}. \tag{36}$$

From Eq. (36), when α approaches zero, the truncation time approaches infinity. When $\alpha\to 1$, the truncation time goes to zero. Thus, the smaller the α is, the longer the system spends for achieving a rare density state.

When a source is taken into consideration, the solution to Eq. (13) can be expressed as in Eq. (33). If $\alpha\to 1$, corresponding to the ordinary diffusion equation, the factor $(t-s)^{\alpha-1}$ in the integrand equals unity, so that this factor does not affect the density profiles. However, since $0<\alpha<1$, this factor cannot be disregarded. Moreover, the factor $B_n(t)(t-s)^{\alpha-1}$ arising from the source term implies that the density profile at position r and time t is influenced by the past history of the source term through the factor $(t-s)^{\alpha-1}$. In other words, the factor $(t-s)^{\alpha-1}$ strengthens the memory effects of the source term. Taking our work as an example, the initial conditions $n(r,0)=0$ and $S_{\rm add=const}$ are assumed, so $A_n=0$ and B_n is independent of time. Therefore, combining Eqs. (28), (32), and (33), we obtain

$$n(r,t)=\sum_{n=1}^{\infty}\frac{2S_{\rm add}}{r_n J_1(r_n)}J_0(r_n r)t^\alpha E_{\alpha,\alpha+1}(-D_\alpha r_n^2 t^\alpha), \tag{37}$$

where we have used the formulae

$$\int_0^1 rJ_0(r_n r)\mathrm{d}r=\frac{J_1(r_n)}{r_n},$$

$$\int_0^t p^{\alpha-1}E_{\alpha,\alpha}(-D_\alpha r_n^2 p^\alpha)\mathrm{d}p=t^\alpha E_{\alpha,\alpha+1}(-D_\alpha r_n^2 t^\alpha).$$

As $t\to\infty$, the system with a source arrives at a steady state, which means that Eq. (37) is a function of radial position and is independent of time. Moreover, from Eq. (35), we have

$$t^\alpha E_{\alpha,\alpha+1}(-D_\alpha r_n^2 t^\alpha)\approx\frac{1}{D_\alpha r_n^2}\left[1-\frac{1}{D_\alpha r_n^2 t^\alpha\Gamma(1-\alpha)}\right].$$

We further assume $D_\alpha r_n^2=1$ so as to study the influence of α on the density profiles, and the above equation becomes

$$t^\alpha E_{\alpha,\alpha+1}(-t^\alpha)\approx 1-\frac{1}{t^\alpha\Gamma(1-\alpha)}. \tag{38}$$

If we make Eq. (38) a function independent of time, i.e., in a steady state, the second term on the right-hand side should be much less than the first term, such that the second term can be ignored. Figure 2(d) shows that the density profile for $\alpha=0.2$ has a larger difference from $n_{\rm s}(r)=(1-r^2)/4$ than that for $\alpha=0.8$, which implies that the value of α determines how long a system needs to reach a steady state. To estimate the truncation time in order to ignore the second term on the right-hand side of Eq. (38), we may assume that the second term is 1% of the first term to obtain another truncation time $t_{\rm trun,s}=[100/\Gamma(1-\alpha)]^{1/\alpha}$ (s in the subscript denotes a steady state). Note that the form of this truncation time is the same as in Eq. (36), but the physical meanings are different. The ratio of $t_{\rm trun,s}$ for $\alpha=0.2$ to that for $\alpha=0.8$ is $t_{\rm trun,s}\big|_{\alpha=0.2}/t_{\rm trun,s}\big|_{\alpha=0.8}\approx 10^8$, which means that the truncation time $t_{\rm trun,s}$ for $\alpha=0.2$ is much greater than that for $\alpha=0.8$. Thus, as α decreases, the time required to reach a steady state increases.

To investigate the evolution of temperature profiles under off-axis heating processes, we assume that the heating source has the form $H_{\rm add}=H_{\rm e}\mathrm{e}^{-(r-r_0)^2/a^2}$, where $r_0=0.75$, $a=0.05$, and $H_{\rm e}$ is a constant, such that

$$2\pi\int_0^1 H_{\rm add}r\mathrm{d}r=2\pi H_{\rm e}\int_0^1\mathrm{e}^{-(r-r_0)^2/a^2}r\mathrm{d}r=1.$$

For theoretical work, we may express the heating source as

$$H_{\rm add}=\frac{\delta(r-r_0)}{2\pi r}. \tag{39}$$

Moreover, the Dirac delta function can be expressed as the derivative of the Heaviside step function

$$\delta(r-r_0)=\frac{\mathrm{d}}{\mathrm{d}r}H(r-r_0).$$

Therefore, we have

$$\begin{aligned}B_n(t)&=\frac{2}{J_1^2(r_n)}\int_0^1 rH_{\rm add}(r,t)J_0(r_n r)\mathrm{d}r\\&=\frac{2}{J_1^2(r_n)}\int_0^1 r\frac{J_0(r_n r)}{2\pi r}\left[\frac{\mathrm{d}}{\mathrm{d}r}H(r-r_0)\right]\mathrm{d}r.\end{aligned}$$

Applying integration by parts and utilizing the boundary condition $T(1,t)=0$, the above equation can be written as

$$B_n(t)=\frac{r_n}{\pi J_1^2(r_n)}\int_{r_0}^1 J_1(r_n r)\mathrm{d}r. \tag{40}$$

Substituting Eq. (39) into Eq. (24) and applying the initial condition $T(r,0)=0$ yield

$$T(r,t)=\sum_{n=1}^{\infty}\frac{r_n}{\pi J_1^2(r_n)}J_0(r_n r)t^{\alpha}E_{\alpha,\alpha+1}(-\chi_\alpha r_n^2 t^{\alpha})\int_{r_0}^{1}J_1(r_n r)\mathrm{d}r. \tag{41}$$

As $t\to\infty$, the solution for the steady state reads

$$T(r)=\sum_{n=1}^{\infty}\frac{1}{\pi J_1^2(r_n)}\frac{J_0(r_n r)}{\chi_\alpha r_n}\int_{r_0}^{1}J_1(r_n r)\mathrm{d}r. \tag{42}$$

Another way to obtain the analytical solution for steady states is to directly solve Eq. (22) and note that $T(r,t)=T(r)$ in a steady state. That is,

$$\frac{\chi_\alpha}{r}\frac{\mathrm{d}}{\mathrm{d}r}\left(r\frac{\mathrm{d}T}{\partial r}\right)=-\frac{1}{2\pi r}\frac{\mathrm{d}}{\mathrm{d}r}H(r-r_0). \tag{43}$$

The solution to Eq. (39) reads

$$T(r)=\frac{H(r-r_0)}{2\pi\chi_\alpha}\ln\left(\frac{r_0}{r}\right)-\frac{\ln r_0}{2\pi\chi_\alpha}. \tag{44}$$

After a plasma system is heated from the edge, the heat starts to be conducted by Fick's law. Therefore, a hollow temperature profile is formed. As time passes, the temperature at the core increases and the hollow profile flattens. When the plasma system is in a steady state, the temperature profile does not evolve with time, consistent with the brown curves in Fig. 5. However, the time required to reach the steady state increases as α decreases. Hence, the smaller the α is, the longer the hollow temperature profile can exist. This can also be concluded from the formula $t_{\mathrm{trun,s}}=[100/\Gamma(1-\alpha)]^{1/\alpha}\to\infty$ for $\alpha\to 0$, implying that as α approaches zero, the system requires an infinite amount of time to reach the steady state and the hollow temperature profile can be observed indefinitely.

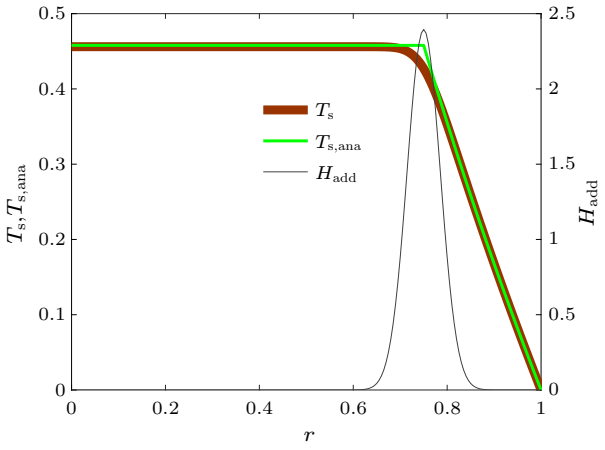


Fig. 5. The temperature profile in a steady state can be numerically calculated through the finite difference scheme as shown by the brown curve denoted as T_s. It can also be analytically derived from Eq. (43), as shown by the green curve denoted as $T_{s,ana}$. The source profile for the numerical calculation has the form $H_{add}=H_e e^{-(r-r_0)^2/a^2}$ instead of the Dirac delta function.

5. Summary and conclusion

In this work, we have investigated the effect of a temporal fractional derivative on transport in a Fickian process with and without sources. The fractional order of the temporal derivative in Eq. (13) can be derived from the CTRW model and the DCT method. Moreover, Eq. (2) states that the time evolution of the density is affected by its past history, which means that the memory effects have a significant influence on anomalous transport. When $\alpha\to 1$, memory effects abate and disappear, reducing the fractional diffusion equation to the ordinary diffusion equation.

When a source term is taken into account, the memory effects have an influence on the time needed to reach a steady state. As shown in Figs. 2 and 3, as α increases, the time required to achieve a steady state decreases. Hence, for a system in a sub-diffusive process with a source, the memory effects will prevent the system from reaching a steady state. Therefore, memory effects could be significant in allowing hollow temperature profiles to exist for a long time under off-axis heating.

It should be pointed out that non-local effects are also important to transport in Markovian processes, as investigated in Refs. [35–38]. It would be interesting to consider both non-local and memory effects at the same time. In addition, the fractional order α depends on the Kubo number $K=\varepsilon\tau_c/(B\lambda_c^2)$, which means that it depends on the magnetic fields and electrostatic fluctuations. In a real tokamak device, the magnetic field has spatial and temporal dependences, which implies that α is a function of space and time. Moreover, as $K\gg 1$ implying weak magnetic field or large electrostatic fluctuations in a system, the memory effects become significant to impede transport processes. Hence, our future work will focus on anomalous transport with spatial-temporal variance of the fractional order α.

Acknowledgments

This work was supported by the National Key R&D Program of China (Grant No. 2022YFE03090000), the National Natural Science Foundation of China (Grant No. 11925501), and the Fundamental Research Fund for the Central Universities (Grant No. DUT22ZD215).

References

[1] Vlad M, Reuss J, Spineanu F and Misguich J 1998 *J. Plasma Phys.* **59** 707
[2] Pommois P, Zimbardo G and Veltri P 2007 *Phys. Plasmas* **14** 012311
[3] Gustafson K, Ricci P, Furno I and Fasoli A 2012 *Phys. Rev. Lett.* **108** 035006
[4] Gustafson K and Ricci P 2012 *Phys. Plasmas* **19** 032304
[5] Bovet A, Fasoli A and Furno I 2014 *Phys. Rev. Lett.* **113** 225001

[6] Zimbardo G, Amato E, Bovet A, Effenberger F, Fasoli A, Fichtner H, Furno I, Gustafson K, Ricci P and Perri S 2015 *J. Plasma Phys.* **81** 495810601

[7] Zarzoso D and del-Castillo-Negrete D 2020 *J. Plasma Phys.* **86** 795860201

[8] Boyd T J M and Sanderson J J 2003 *The Physics of Plasmas (New York: Cambridge University Press)* p. 301

[9] Guthrie A and Wakerling R 1949 *The Characteristics of Electrical Discharges in Magnetic Fields* (New York: McGraw-Hill) p. 58

[10] Taylor J B and McNamara B 1971 *Phys. Fluids* **14** 1492

[11] Hsu J Y, Wu K B, Agarwal S K and Ryu C M 2013 *Phys. Plasmas* **20** 062302

[12] Balescu R 2005 *Aspects of Anomalous Transport in Plasmas* (Boca Raton: CRC Press)

[13] Vlad M, Spineanu F, Misguich J H and Balescu R 1998 *Phys. Rev. E* **58** 7359

[14] Vlad M, Spineanu F, Misguich J H and Balescu R 2002 *Nucl. Fusion* **42** 157

[15] Negrea M 2020 *Plasma Sci. Technol.* **22** 015101

[16] Crotinger J A and Dupree T H 1992 *Phys. Fluids B* **4** 2854

[17] Balescu R 2000 *Plasma Phys. Control. Fusion* **42** B1

[18] Samko S G, Kilbas A A and Marichev O I 1993 *Fractional Integrals and Derivatives: Theory and Applications* (Amsterdam: Gordon and Breach Science Publishers)

[19] Podlubny I 1999 *Fractional Differential Equations* (San Diego: Academic Press)

[20] Kilbas A A, Srivastava H M and Trujillo J J 2006 *Theory and Applications of Fractional Differential Equations* (Netherlands: Elsevier)

[21] Caputo M 1967 *Geophys. J. R. Astronom. Soc.* **13** 529

[22] Oldham K B and Spanier J 1974 *The Fractional Calculus: Theory and Applications of Differentiation and Integration to Arbitrary Order* (New York: Academic Press) p. 140

[23] Li C, Deng W H and Wu Y J 2011 *Comput. Math. Appl.* **62** 1024

[24] Gao G H, Sun Z Z and Zhang H W 2014 *J. Comput. Phys.* **259** 33

[25] He S B, Wang H H and Sun K H 2022 *Chin. Phys. B* **31** 060501

[26] Povstenko Y Z 2008 *J. Mol. Liq.* **137** 46

[27] Povstenko Y Z 2009 *Quart. Appl. Math.* **67** 113

[28] Povstenko Y Z 2012 *Arch. Appl. Mech.* **82** 345

[29] Qi H T and Liu J G 2010 *Meccanica* **45** 577

[30] Povstenko Y 2013 *Eur. Phys. J. Spec. Top.* **222** 1767

[31] Chung W S, Gungor A, Kříž J, Lütfüoğlu B C and Hassanabadi H 2023 *Chin. Phys. B* **32** 040202

[32] Montroll E W and Weiss G H 1965 *J. Math. Phys.* **6** 167

[33] Sánchez R and Newman D 2018 *A Primer on Complex Systems: With Applications to Astrophysical and Laboratory Plasmas* (Netherlands: Springer) p. 243

[34] Mantica P, Gorini G, Hogeweij G M D, Lopes Cardozo N J and Schilham A M R 2000 *Phys. Rev. Lett.* **85** 4534

[35] Kullberg A, del-Castillo-Negrete D, Morales G J and Maggs J E 2013 *Phys. Rev. E* **87** 052115

[36] Kullberg A B 2014 *Non-local fractional diffusion and transport in magnetized plasmas* (PhD Dissertation) (Los Angeles: University of California)

[37] Kullberg A, Morales G J and Maggs J E 2014 *Phys. Plasmas* **21** 032310

[38] Wu K B, Wei L and Wang Z X 2022 *Plasma Sci. Technol.* **24** 045101